Applied Physics Letters

RESEARCH ARTICLE | MAY 05 2026

Super-resolution imaging of azimuthal features with illumination carrying OAM

Nilakshi Senapati ; Abhinandan Bhattacharjee ; Kedar Khare ; Anand K. Jha

Appl. Phys. Lett. 128, 181107 (2026)
https://doi.org/10.1063/5.0319922

Applied Physics Letters ARTICLE pubs.aip.org/aip/apl

Super-resolution imaging of azimuthal features with illumination carrying OAM

Cite as: Appl. Phys. Lett. **128**, 181107 (2026); doi: 10.1063/5.0319922
Submitted: 27 December 2025 · Accepted: 15 April 2026 ·
Published Online: 5 May 2026

Nilakshi Senapati,[1,a)] Abhinandan Bhattacharjee,[2] Kedar Khare,[3] and Anand K. Jha[1,a)]

AFFILIATIONS

[1]Department of Physics, Indian Institute of Technology Kanpur, Kanpur, Uttar Pradesh 208016, India
[2]Institute for Photonic Quantum Systems (PhoQS), Paderborn University, Warburger Str. 100, 33098 Paderborn, Germany
[3]Optics and Photonics Centre, Indian Institute of Technology Delhi, New Delhi 110016, India

[a)]Authors to whom correspondence should be addressed: nilakshisenapati0408@gmail.com and akjha@iitk.ac.in

ABSTRACT

Super-resolution imaging refers to imaging techniques that surpass the Rayleigh resolution limit. One standard way to achieve super-resolution is by structuring the phase of the field illuminating the object. Although super-resolution techniques are already employed in commercial imaging devices, intense research efforts continue to enhance the resolution even further. In this work, we show that if the field illuminating the object is structured in the azimuthal coordinate—such as a field carrying orbital angular momentum (OAM)—the azimuthal features of the object can be imaged with enhanced imaging resolution. We experimentally demonstrate it with two objects, namely, an azimuthal double-slit and a Siemens star. We find that for a given azimuthal feature, there is an optimum OAM mode index of the illumination that gives the best imaging resolution. Super-resolution imaging of azimuthal features can have important implications, especially for some biological objects that are known to have predominantly azimuthal features.

The maximum imaging resolution that an imaging system can achieve is known as the Rayleigh resolution[1] criterion. Enhancing resolution beyond the Rayleigh resolution limit is referred to as super-resolution,[2,3] and it has been a very active area of research in the last few decades with the invention of techniques such as stimulated emission depletion microscopy (STED),[4,5] structured illumination microscopy (SIM),[6,7] spatial-mode demultiplexing (SPADE),[8,9] and Fourier ptychography (FT).[10] Among these techniques, STED[4,5] and SIM[6,7] use spatially coherent illumination but collect incoherent fluorescence. SPADE[8,9] uses incoherent illumination but collects spatially coherent light modes, while in FT[10] the illumination and collection involve coherent light.

Another very active area of research in recent decades has been light fields carrying orbital angular momentum (OAM).[11,12] Such fields have emerged as powerful tools in areas such as long-distance communication,[13–15] increased error tolerance in quantum communication,[16,17] gate implementation,[18,19] propagation through turbulence,[20] quantum metrology,[21] angular momentum transfer,[22] rotational Doppler effect,[23,24] and fundamental tests of quantum mechanics.[25–27] Light fields carrying OAM have also been used for edge imaging[28,29] and for fluorescence imaging such as STED microscopy.[4,5] Furthermore, it has been shown that when light coming from two spatially separated point sources is made to go through an OAM imparting forked hologram, one can resolve the two sources at an angular separation one order of magnitude below the Rayleigh criterion.[30]

However, the use of OAM modes for direct super-resolution imaging has been very limited, and most of the works have been related to theoretical modeling and numerical simulations.[31–34] These works hint at the super-resolution-imaging potential of fields carrying OAM modes but do not point out the unique and optimum use of such fields for enhancing the imaging resolution. Furthermore, there has been no experimental demonstration in direct imaging of super-resolution with illumination carrying OAM. In this work, we report experimental demonstrations of super-resolution imaging with illumination carrying OAM. We find that the unique benefit of illumination carrying OAM is in super-resolving the azimuthal features of an object and that if the object has predominantly non-azimuthal features, the OAM modes are not the optimum illumination for achieving super-resolution. We also derive the mathematical relation for the optimal OAM mode for a given azimuthal feature.

Figure 1 shows imaging configurations with various objects and illuminations. We use these to illustrate how structuring the wavefront of the illumination affects imaging resolution. In every

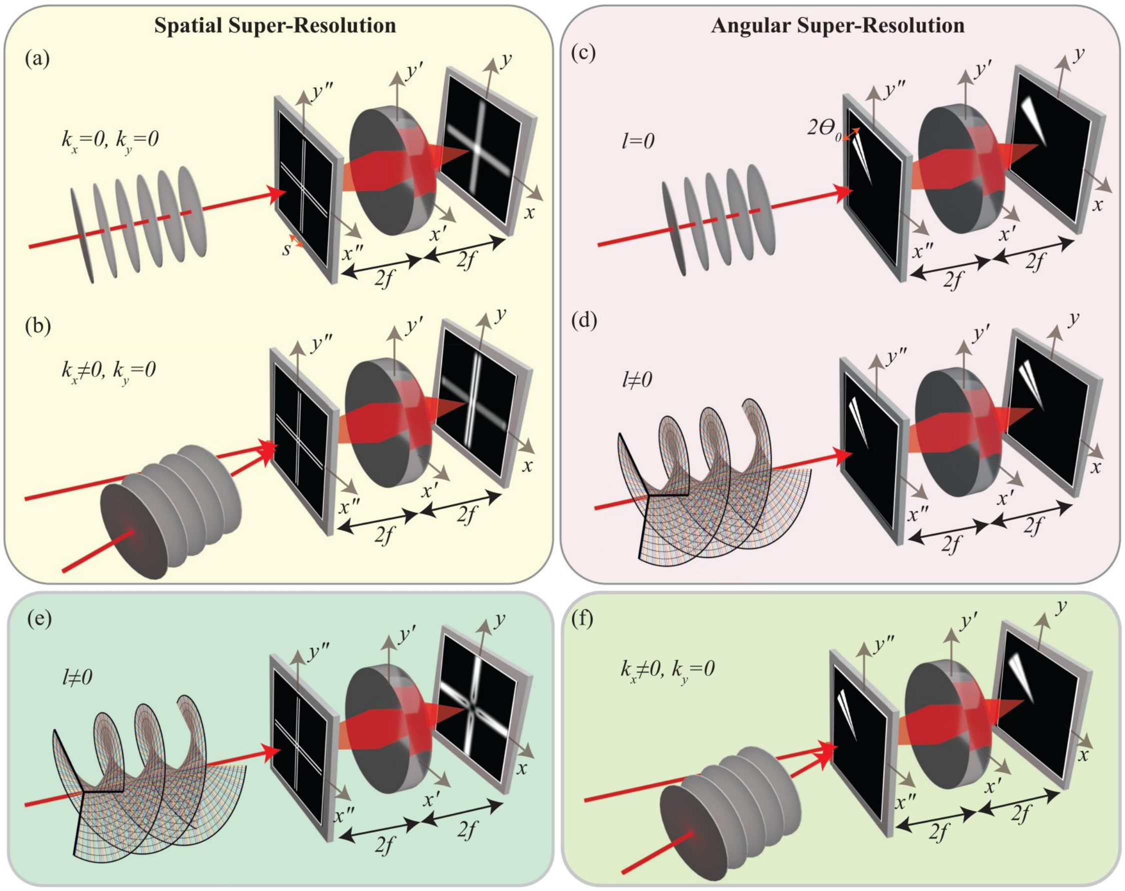

FIG. 1. Illustrating how structuring the wavefront of the illumination in a particular coordinate helps super-resolve the object features in that coordinate. The object present in (a), (b), and (e) is in the form of a transverse double-slit, with two slits in both *x*- and *y*-directions. The slit width and slit separation of the object are 0.0625 and 0.125 mm, respectively. The object present in (c), (d), and (f) is an azimuthal double-slit, with the angular slit width being 0.02π and the angular slit separation being 0.1π. The focal length of the lens is 400 mm. For each figure, we have explicitly shown the transmission function of the object at $z = 0$ and the corresponding image-plane intensity at $z = 4f$ calculated numerically using Eq. (1).

configuration of Fig. 1, the object is placed at $z = 0$, the imaging lens at $z = 2f$, and the image plane is located at $z = 4f$, where f is the focal length of the lens. The electric field at $z = 0$ plane is given by $E(x'', y''; z = 0) = E_{\rm in}(x'', y''; z = 0)T(x'', y'')$, where $E_{\rm in}(x'', y''; z = 0)$ is the illumination field and $T(x'', y'')$ is the object transmission function. This field undergoes Fresnel propagation from $z = 0$ plane to the lens plane ($z = 2f$), where it acquires the quadratic phase due to the lens and then further propagates to the image plane. Therefore, the electric field at $z = 4f$ becomes (see supplementary material Secs. I A and 5.3 of Ref. 35)

$$E(x, y; z = 4f) = e^{-\frac{ik}{4f}(x^2+y^2)} \iint E_{\rm in}(x'', y'', z = 0) \times T(x'', y'') e^{\frac{ik}{4f}(x''^2+y''^2)} e^{-\frac{k^2d^2}{4f^2}(x+x'')^2} e^{-\frac{k^2d^2}{4f^2}(y+y'')^2} dx''dy'',$$

where d is the radius of the lens aperture. The image-plane intensity $I(x, y, z = 4f) = |E(x, y, z = 4f)|^2$ then becomes

$$I(x, y, z = 4f) = e^{-\frac{x^2+y^2}{\sigma_p^2}} \left| \iint E_{\rm in}(x'', y'', z = 0) T(x'', y'') \times \exp\left[-\frac{(x''^2 + y''^2)}{2\sigma_p^2}\left(1 - i\frac{k\sigma_p^2}{2f}\right)\right] \exp\left[-\frac{xx'' + yy''}{\sigma_p^2}\right] dx''dy'' \right|^2, \qquad (1)$$

where $\sigma_p = \frac{2f}{kd}$. The objects present in the left column of figures in Fig. 1 are in the form of a transverse double-slit, with a double-slit in both *x*- and *y*-directions. The object present in the right column of figures is an azimuthal double-slit. For the transverse-double-slit object, we take the slit width and slit separation to be 0.0625 and 0.125 mm, respectively. For the azimuthal-double-slit object, we take the angular width to be 0.02π and the angular slit separation to be 0.1π. For each figure in Fig. 1, we have explicitly shown the transmission function of the object at the $z = 0$ plane and the corresponding image-plane intensity calculated numerically using Eq. (1) at the $z = 4f$ plane. For all the numerical calculations, we have taken $d = 2.5\,\text{mm}$, $f = 400\,\text{mm}$, and $\lambda = 633\,\text{nm}$. We note that the values of the various object and illumination parameters have been chosen such that the object features cannot be resolved under the plane wave illumination—this is to highlight the effect of structured illumination on enhancing image resolution that we next demonstrate. We show that structuring the illumination in a particular coordinate leads to super-resolution of the object features in that coordinate.

Figures 1(a) and 1(b) depict imaging of a transverse double-slit object when the illumination is by a plane wave ($k_x = k_y = 0$) and a plane wave tilted in x-direction ($k_x \neq 0; k_y = 0$), respectively. We find that the plane wave illumination is not able to resolve the object. However, the tilted plane wave is able to super-resolve the two slits in the x-direction but not in the y-direction. This is because the phase of the titled plane wave changes as $k_x x$, which structures the phase in the x-direction but not in the y-direction, leading to super-resolution only in the x-direction. It can be shown that one obtains optimum super-resolution when the phase of the illuminating field at the two slit locations differs by π[2,36–39] (see supplementary material Sec. I E for more detailed explanation). This result can be extended to derive a relation between the slit separation s and the optimum k_x for super-resolution. The relationship is given by $k_x s = (2n+1)\pi$ (see supplementary material Sec. I B for more details). For example, the Hermite–Gaussian ($\text{HG}_{1,1}$) mode can provide a natural and effective approach for achieving super-resolution of a spatial double-slit object, as it has a π phase jump around the center. Figure 1(c) depicts imaging of the azimuthal-double-slit object illuminated by a field carrying no OAM ($l = 0$), while in Fig. 1(d) the illuminating field carries finite OAM ($l \neq 0$). We find that while the $l = 0$ illumination is not able to resolve the object, the illumination carrying non-zero OAM leads to super-resolution. Again, this is because the phase of an OAM carrier is structured as $l\theta$, and it, therefore, leads to super-resolution of azimuthal features.

Figure 1(e) depicts imaging of the transverse-double-slit object illuminated with a field carrying OAM. Although the resolution in this case is better than that with the plane wave, it is worse compared to resolution with the tilted plane wave depicted in Fig. 1(c). Similarly, Fig. 1(f) depicts imaging of the azimuthal-double-slit object illuminated with the tilted plane wave. Again, in this case, although the resolution is better than that with a beam carrying no OAM, it is worse compared to the resolution with an OAM carrying field, as depicted in Fig. 1(d). Thus, for direct imaging, structuring the illumination does not lead to super-resolution of every object feature. For the optimum super-resolution imaging of a given object feature, the illumination needs to be structured accordingly. This fact could be utilized in proposals[31–34] in which OAM carrying illumination is employed for super-resolution of every object features. If the light is structured in the x-direction, it can lead to optimal resolution enhancement only in the x-direction. Similarly, for optimal super-resolution of the azimuthal features, the illumination needs to be structured in the azimuthal direction.

So far, through the numerical simulations of Eq. (1), we have shown that the fields carrying OAM lead to super-resolution of azimuthal features. In what follows, we derive a relation for the optimum modes l_{opt} that best resolves an azimuthal feature, namely, the angular separation in an azimuthal double-slit. To this end, we express the image-plane intensity of Eq. (1) in the polar coordinates by using the transformation: $(x, y) = (r\cos\theta, r\sin\theta)$ and $(x'', y'') = (r''\cos\theta'', r''\sin\theta'')$. We take $E_{\text{in}}(x'', y'', z = 0) \to E_{\text{in}}(r'', \theta'', z = 0) = \exp[-\frac{r''^2}{4w^2}]e^{il\theta''}$ where w is the beam waist of the field and l is the OAM mode index. The object is taken to have only the azimuthal feature, that is, $T(r'', \theta'') = T(\theta'')$. Equation (1) thus becomes

$$I(r, \theta, z = 4f) = Ae^{\left(-\frac{r^2}{\sigma_p^2}\right)}\left|\iint T(\theta'')e^{il\theta''}\exp\left[-\frac{ar''^2}{2\sigma_p^2}\right] \times \exp\left[-\frac{r''r}{\sigma_p^2}\cos(\theta-\theta'')\right]r''dr''d\theta''\right|^2, \tag{2}$$

where $a = 1 + \frac{\sigma_p^2}{2w^2} - i\frac{k\sigma_p^2}{2f}$. Next, we consider an azimuthal-double-slit object of infinitesimally narrow slit width and angular separation of $2\theta_0$ such that the transmission function is given by $T(\theta'') = \delta(\theta''-\theta_0) + \delta(\theta''+\theta_0)$. For this object, the image-plane intensity $I(r, \theta, z = 4f)$ can be expressed as

$$\begin{aligned} I(r,\theta,z=4f) &= Ae^{-\frac{r^2}{\sigma_p^2}}\left|\iint[\delta(\theta''-\theta_0)+\delta(\theta''+\theta_0)] \times e^{il\theta''}\exp\left[-\frac{ar''^2}{2\sigma_p^2}\right]\exp\left[-\frac{r''r}{\sigma_p^2}\cos(\theta-\theta'')\right]r''dr''d\theta''\right|^2 \\ &= |f(r,\theta-\theta_0)e^{il\theta_0}+f(r,\theta+\theta_0)e^{-il\theta_0}|^2, \end{aligned} \tag{3}$$

where

$$f(r, \theta) = Ae^{-\frac{r^2}{2\sigma_p^2}}\int\exp\left[-\frac{ar''^2}{2\sigma_p^2}\right]\exp\left[-\frac{r''r}{\sigma_p^2}\cos\theta\right]r''dr''. \tag{4}$$

Now, at $\theta = 0$, that is, at the mid-point between the two slits, the intensity $I(r, \theta, z = 4f)$ is given by

$$I(r, \theta = 0, z = 4f) = |f(r, -\theta_0)|^2 + |f(r, \theta_0)|^2 + 2f(r, -\theta_0)f(r, \theta_0)\cos 2l\theta_0. \tag{5}$$

Here, we have assumed the function $f(r, \theta)$ to be real. Now, taking $f(r, -\theta_0) = f(r, \theta_0) = f_0$, we obtain

$$I(r, \theta = 0, z = 4f) = 2|f_0|^2(1 + \cos 2l\theta_0). \tag{6}$$

For the maximum image contrast, we have to have $I(r, \theta = 0, z = 4f) = 0$. This condition is satisfied when $\cos 2l\theta_0 = -1$, which gives the optimum OAM mode index l_{opt} at which the contrast is maximum

$$l_{\text{opt}} = \frac{(2n+1)\pi}{2\theta_0}, \tag{7}$$

where $n = 0, \pm1, \pm2, \ldots$ (see supplementary material Sec. I C for more details of the above calculations). The observed resolution enhancement originates from the relative phase difference between the fields incident on adjacent slits, which governs the interference in the intermediate region. This contribution is captured by the third term in Eq. (5). As the phase difference increases from 0 to π, the resolution progressively improves, reaching maximum contrast at π, where complete destructive interference yields 100% visibility. In this framework, the relative phase is given by $\Delta\phi = 2l\theta_0$ (see supplementary material Sec. I E for detailed explanation). The smallest OAM mode index at which the contrast becomes maximum is given by $\frac{\pi}{2\theta_0}$. We note that when the illuminating field is a plane wave ($l = 0$), instead of an OAM carrying field, we obtain $I(r, \theta = 0,\ z = 4f) = 4|f_0|^2$. The contrast and, hence, resolution in this case is much worse—this has been illustrated through Figs. 1(c) and 1(d). We further note that if the illumination is azimuthally incoherent, instead of being coherent, the cosine term in Eq. (6) becomes zero giving $I(r, \theta = 0, z = 4f) = 2|f_0|^2$. The resolution with incoherent light defines the Rayleigh resolution limit. Thus, we see that the imaging contrast with a plane wave is worse than the Rayleigh resolution limit while with an OAM carrying field it surpasses the Rayleigh limit (see supplementary material Sec. I D for details).

Figure 2(a) shows the experimental setup. A helium–neon (He–Ne) laser at 633 nm is used as a light source. The laser is spatially filtered in order to generate a high-quality Gaussian beam which is then made to fall onto the spatial light modulator (SLM) to generate fields with different OAM mode index by displaying the corresponding holograms on the SLM.[40] Here, a half-wave plate is used to rotate the incident polarization to match the operating polarization of the SLM,[41] ensuring efficient phase modulation. The SLM is kept at $z = 0$, the lens at $z = 2f$ and the CCD camera at $z = 4f$. In addition to generate the illumination, the SLM also holds the objects. The objects are displayed on the SLM and then imaged onto the multipixel CCD camera using a lens of focal length $f = 400$ mm in a 1:1 conjugate. The aperture size of the lens is kept at $d = 2.5$ mm to keep the numerical aperture of the imaging system such that the plane wave illumination is not able to resolve the objects. We use two separate objects with only azimuthal features. The first one is an azimuthal double-slit as shown in Fig. 2(b) and the other one is the Siemens star as shown in Fig. 2(c). For both the objects, the angular slit width is 0.02π and the angular slit separation ($2\theta_0$) is 0.1π. We note that in our experiments, we use Laguerre–Gaussian modes. Although these modes have $e^{il\theta}$ dependence, the intensity distribution is non-uniform in the radial direction with a null in the center of the beam. To obtain fields with nearly uniform radial intensity and an $e^{il\theta}$ phase dependence, we superpose Laguerre–Gaussian modes with varying beam waists while keeping the OAM mode index l fixed. For the Siemens star object (Fig. 4), the high density of angular features near the center introduces noticeable aliasing due to SLM's pixelation effect during beam waist scanning; therefore, the central region within a certain radius is excluded from the analysis to ensure a clear interpretation of the resolution behavior.

For the object in Fig. 2(b), the measured image intensities are presented in Fig. 3(a) for various OAM modes index l of the illumination. To quantify the resolution enhancement, we use visibility of images in the following manner. First, using the expression in Eq. (1), we calculate the radially averaged intensity given by

$$I(\theta) = \int rI(r, \theta, z = 4f)dr. \tag{8}$$

We then define the visibility as $V = \frac{I(\theta)_{\max} - I(\theta)_{\min}}{I(\theta)_{\max} + I(\theta)_{\min}}$. We measure V as a function of l and indicate that on each plot in Fig. 3(b). We find that field with $l = 0$ is not able to resolve the azimuthal double-slit. However, the resolution improves with increasing l, reaching the maximum visibility at $l_{\text{opt}} = 10$, verifying the relation given in Eq. (7) for $n = 0$. At this point, the relative phase difference ($\Delta\phi$) between two adjacent slit locations becomes $2l\theta_0 = \pi$, ensuring the perfect destructive interference. When the OAM is increased beyond $l = 10$, the visibility decreases reaching its minimum value at $l = 20$ and then returns to its maximum at $l = 30$ as the destructive interference condition is achieved at all $2l\theta_0 = (2n + 1)\pi$, where $n = 0, 1, 2, \ldots$. For the given setup, the Rayleigh criterion gives a minimum azimuthal separation of $\pi/8 \approx 0.12\pi$. However, using our present technique which we refer as OAM-based azimuthal super-resolution imaging scheme (OASIS), we achieve $\pi/10 \approx 0.1\pi$ with nearly 100% visibility (see supplementary material Sec. I D for details). This demonstrates sub-Rayleigh resolution with nearly an order-of-magnitude improvement in visibility, enabling high-contrast imaging beyond the diffraction limit.

For the object in Fig. 2(c), the measured image intensities are presented in Fig. 4(a) for various OAM modes index l of the illumination. We measure V as a function of l and present the results in Fig. 4(b). We find that unlike the plots in Fig. 3(b), these plots have more experimental noise. Therefore, for quantifying the azimuthal resolution in this case, in addition to measuring the visibility, we also

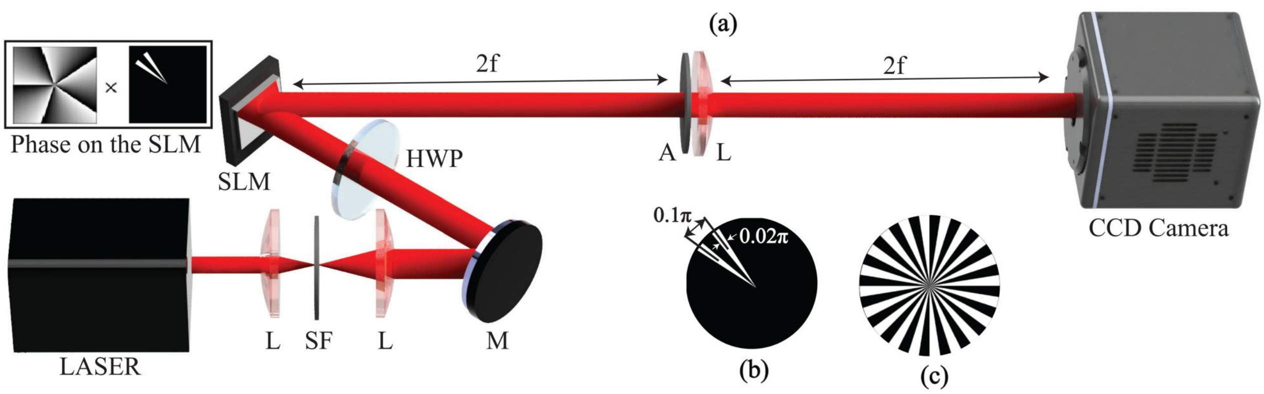

FIG. 2. (a) Schematic of the experimental setup. (b) The azimuthal-double-slit object. (c) The Siemens star object. For the objects shown in (b) and (c), the angular slit width is 0.02π and the angular slit separation is 0.1π. SF: spatial filter, HWP: half-wave plate, SLM: spatial light modulator, A: aperture, L: lens, M: mirror.

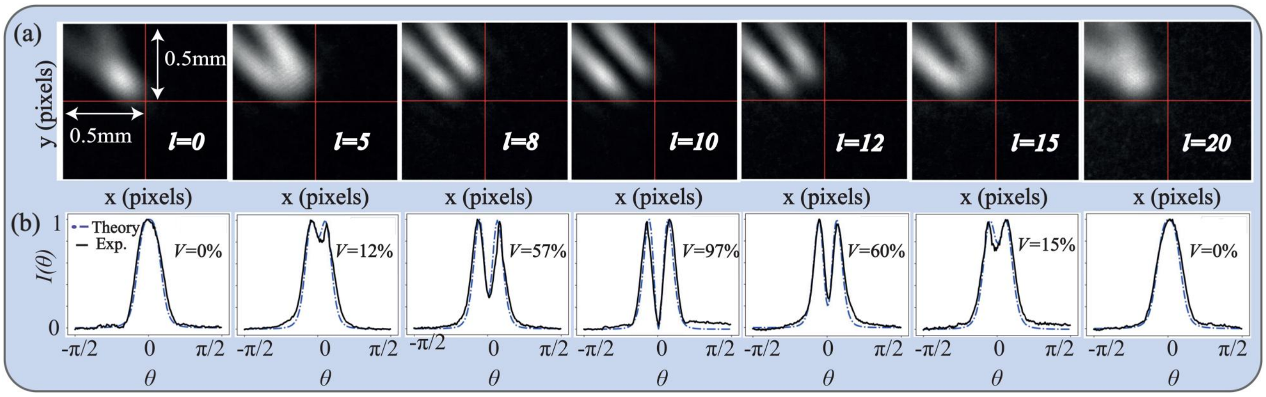

FIG. 3. Experimental results. (a) Image intensity $I(r, \theta, z = 4f)$ of the azimuthal-double-slit object shown in Fig. 2(b) for various OAM mode index l of the illumination. (b) The plot of the radially averaged intensity $I(\theta)$, defined in Eq. (8), as a function of θ for various plots shown in (a). The visibility V of the intensity pattern $I(\theta)$ is indicated on each plot.

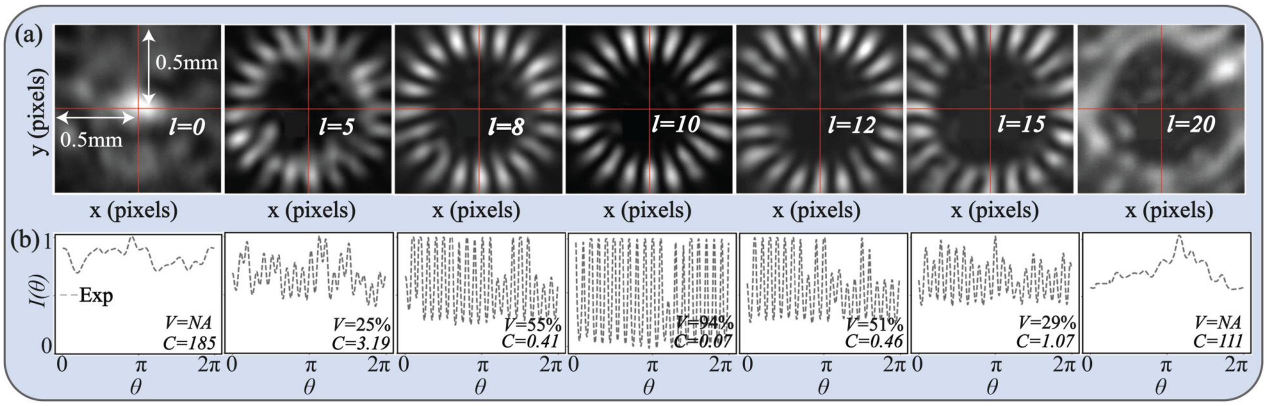

FIG. 4. Experimental results. (a) Image intensity $I(r, \theta, z = 4f)$ of the Siemens star object shown in Fig. 2(c) for various OAM mode index l of the illumination. (b) The plot of the radially averaged intensity $I(\theta)$, defined in Eq. (8), as a function of θ for various plots shown in (a). The visibility V of the intensity pattern $I(\theta)$ and the Cramér–Rao Lower Bound C are indicated on each plot.

evaluate the Fisher Information (FI) and take the corresponding Cramér–Rao Lower Bound (CRLB) C[42,43] as a suitable metric (see supplementary material Sec. II for more details). We note that a smaller value for C implies better imaging resolution. Both V and C are indicated on each plot in Fig. 4(b). We clearly see that C is lowest for $l = 10$, indicating optimum super-resolution and verifying the relation given in Eq. (7) for $2\theta_0 = 0.1\pi$.

In summary, in this work, we show that if the field illuminating the object is structured in the azimuthal coordinate—such as a field carrying orbital angular momentum (OAM)—the azimuthal features of an object can be imaged with enhanced resolution. We experimentally demonstrate it with two objects, namely, an azimuthal double-slit and a Siemens star. We find that for a given azimuthal feature, there is an optimal OAM mode index of the illumination that gives the best resolution. Being able to image azimuthal features with enhanced resolution can have important implications for objects with predominantly azimuthal features, such as the centrosome in animal cells.[44]

See the supplementary material for expanded mathematical derivations, including intermediate steps, standard definitions, and discussions.

N.S. thanks the Prime Minister's Research Fellowship (PMRF), Government of India, for financial support. We acknowledge financial support from the Science and Engineering Research Board through Grant Nos. STR/2021/000035 and CRG/2022/003070 and from the Department of Science and Technology, Government of India through Grant No. DST/ICPS/QuST/Theme-1/2019 and through the National Quantum Mission (NQM).

AUTHOR DECLARATIONS

Conflict of Interest

The authors have no conflicts to disclose.

Author Contributions

Nilakshi Senapati: Conceptualization (equal); Data curation (lead); Formal analysis (equal); Investigation (lead); Methodology (equal); Software (lead); Visualization (lead); Writing – original draft (equal); Writing – review & editing (equal). **Abhinandan Bhattacharjee:** Conceptualization (equal); Formal analysis (supporting); Investigation (supporting); Methodology (supporting); Writing – review & editing (equal). **Kedar Khare:** Conceptualization (supporting); Investigation (supporting); Methodology (supporting); Writing – review & editing (supporting). **Anand K. Jha:** Conceptualization (equal); Formal analysis (equal); Funding acquisition (lead); Investigation (equal); Methodology (equal); Project administration (lead); Resources (lead); Supervision (lead); Visualization (equal); Writing – original draft (equal); Writing – review & editing (equal).

DATA AVAILABILITY

The data that support the findings of this study are available on request from the corresponding authors.

REFERENCES

[1] M. Born and E. Wolf, *Principles of Optics: Electromagnetic Theory of Propagation, Interference and Diffraction of Light*, 7th ed. (Cambridge University Press, 1999).
[2] J. W. Goodman, *Statistical Optics* (Wiley-Interscience, New York, 1985), Vol. 1, p. 567.
[3] J. Mertz, *Introduction to Optical Microscopy*, 2nd ed. (Cambridge University Press, 2019).
[4] S. W. Hell and J. Wichmann, "Breaking the diffraction resolution limit by stimulated emission: Stimulated-emission-depletion fluorescence microscopy," Opt. Lett. **19**, 780–782 (1994).
[5] T. A. Klar and S. W. Hell, "Subdiffraction resolution in far-field fluorescence microscopy," Opt. Lett. **24**, 954–956 (1999).
[6] R. Heintzmann, T. M. Jovin, and C. Cremer, "Saturated patterned excitation microscopy—A concept for optical resolution improvement," J. Opt. Soc. Am. A **19**, 1599–1609 (2002).
[7] M. G. L. Gustafsson, "Nonlinear structured-illumination microscopy: Wide-field fluorescence imaging with theoretically unlimited resolution," Proc. Natl. Acad. Sci. U. S. A. **102**, 13081–13086 (2005).
[8] C. Rouvière, D. Barral, A. Grateau, I. Karuseichyk, G. Sorelli, M. Walschaers, and N. Treps, "Ultra-sensitive separation estimation of optical sources," Optica **11**, 166–170 (2024).
[9] M. Tsang, R. Nair, and X.-M. Lu, "Quantum theory of superresolution for two incoherent optical point sources," Phys. Rev. X **6**, 031033 (2016).
[10] G. Zheng, R. Horstmeyer, and C. Yang, "Wide-field, high-resolution Fourier ptychographic microscopy," Nat. Photonics **7**, 739–745 (2013).
[11] L. Allen, M. W. Beijersbergen, R. J. C. Spreeuw, and J. P. Woerdman, "Orbital angular momentum of light and the transformation of Laguerre-Gaussian laser modes," Phys. Rev. A **45**, 8185–8189 (1992).
[12] M. J. Padgett, "Orbital angular momentum 25 years on [invited]," Opt. Express **25**, 11265–11274 (2017).
[13] J. Wang, J.-Y. Yang, I. M. Fazal, N. Ahmed, Y. Yan, H. Huang, Y. Ren, Y. Yue, S. Dolinar, M. Tur, and A. E. Willner, "Terabit free-space data transmission employing orbital angular momentum multiplexing," Nat. Photonics **6**, 488–496 (2012).
[14] Ş. Suciu, G. A. Bulzan, T.-A. Isdrailă, A. M. Pălici, S. Ataman, C. Kusko, and R. Ionicioiu, "Quantum communication networks with optical vortices," Phys. Rev. A **108**, 052612 (2023).
[15] Y. Yan, G. Xie, M. P. J. Lavery, H. Huang, N. Ahmed, C. Bao, Y. Ren, Y. Cao, L. Li, Z. Zhao, A. F. Molisch, M. Tur, M. J. Padgett, and A. E. Willner, "High-capacity millimetre-wave communications with orbital angular momentum multiplexing," Nat. Commun. **5**, 4876 (2014).
[16] N. J. Cerf, M. Bourennane, A. Karlsson, and N. Gisin, "Security of quantum key distribution using *d*-level systems," Phys. Rev. Lett. **88**, 127902 (2002).
[17] G. M. Nikolopoulos, K. S. Ranade, and G. Alber, "Error tolerance of two-basis quantum-key-distribution protocols using qudits and two-way classical communication," Phys. Rev. A **73**, 032325 (2006).
[18] T. C. Ralph, K. J. Resch, and A. Gilchrist, "Efficient Toffoli gates using qudits," Phys. Rev. A **75**, 022313 (2007).
[19] B. P. Lanyon, M. Bibieri, M. P. Almeida, T. Jennewein, T. C. Ralph, K. J. Resch, G. J. Pryde, J. L. O'Brien, A. Gilchrist, and A. G. White, "Simplifying quantum logic using higher-dimensional Hilbert spaces," Nat. Phys. **5**, 134–140 (2009).
[20] A. Bhattacharjee, M. K. Joshi, S. Karan, J. Leach, and A. K. Jha, "Propagation-induced revival of entanglement in the angle-OAM bases," Sci. Adv. **8**, eabn7876 (2022).
[21] A. K. Jha, G. S. Agarwal, and R. W. Boyd, "Supersensitive measurement of angular displacements using entangled photons," Phys. Rev. A **83**, 053829 (2011).
[22] O. Emile and J. Emile, "Optical orbital angular momentum transfer to electronic currents," New J. Phys. **25**, 123055 (2023).
[23] O. Emile and J. Emile, "OAM of light: Origins and applications," Encyclopedia **5**, 152 (2025).
[24] M. P. J. Lavery, S. M. Barnett, F. C. Speirits, and M. J. Padgett, "Observation of the rotational Doppler shift of a white-light, orbital-angular-momentum-carrying beam backscattered from a rotating body," Optica **1**, 1–4 (2014).
[25] D. Kaszlikowski, P. Gnaciński, M. Żukowski, W. Miklaszewski, and A. Zeilinger, "Violations of local realism by two entangled *N*-dimensional systems are stronger than for two qubits," Phys. Rev. Lett. **85**, 4418–4421 (2000).
[26] D. Collins, N. Gisin, N. Linden, S. Massar, and S. Popescu, "Bell inequalities for arbitrarily high-dimensional systems," Phys. Rev. Lett. **88**, 040404 (2002).
[27] A. C. Dada, J. Leach, G. S. Buller, M. J. Padgett, and E. Andersson, "Experimental high-dimensional two-photon entanglement and violations of generalized Bell inequalities," Nat. Phys. **7**, 677–680 (2011).
[28] S. Fürhapter, A. Jesacher, S. Bernet, and M. Ritsch-Marte, "Spiral phase contrast imaging in microscopy," Opt. Express **13**, 689–694 (2005).
[29] J. Zeng, Y. Dong, Y. Wang, J. Zhang, and J. Wang, "Optical imaging using orbital angular momentum: Interferometry, holography and microscopy," J. Lightwave Technol. **41**, 2025–2040 (2023).
[30] F. Tamburini, G. Anzolin, G. Umbriaco, A. Bianchini, and C. Barbieri, "Overcoming the Rayleigh criterion limit with optical vortices," Phys. Rev. Lett. **97**, 163903 (2006).
[31] L. Li and F. Li, "Beating the Rayleigh limit: Orbital-angular-momentum-based super-resolution diffraction tomography," Phys. Rev. E **88**, 033205 (2013).
[32] T. Yang, H. Shi, J. Guo, D. Liu, and Z. Qiao, "Super-resolution performance studies for orbital-angular-momentum-based imaging radar," Int. J. Remote Sens. **42**, 8185–8206 (2021).
[33] M. Ashrafian and L. Yousefi, "Subwavelength imaging using orbital angular momentum waves generated by metasurfaces," Sci. Rep. **15**, 20539 (2025).
[34] B. Liang, F. Shen, S. M. Wang, Y. Zhou, Y. Yang, K. Cheng, G. Zhang, Y. Zheng, Q. H. Liu, and Y. Gong, "Reconstruction of three-dimensional objects in layered composite structures from multimode orbital angular momentum," Phys. Rev. E **105**, 025302 (2022).
[35] J. W. Goodman, *Introduction to Fourier Optics*, 3rd ed. (Roberts & Co. Publishers, 2005).
[36] Z. Marcet, J. W. Paster, D. W. Carr, J. E. Bower, R. A. Cirelli, F. Klemens, W. M. Mansfield, J. F. Miner, C. S. Pai, and H. B. Chan, "Controlling the phase delay of light transmitted through double-layer metallic subwavelength slit arrays," Opt. Lett. **33**, 1410–1412 (2008).
[37] C.-W. Liang, C.-F. Ou, and J. Sasian, "Phase shifting grating-slit test with a cross slit," Opt. Lett. **35**, 496–498 (2010).
[38] C. Ferreira, L. Marinho, T. Brazil, L. Cabral, J. de Oliveira, Jr., M. Sampaio, and I. da Paz, "Gouy phase and visibility in the double-slit experiment," Ann. Phys. **362**, 473–481 (2015).
[39] E. Pietersoone, J. M. Létang, S. Rit, E. Brun, and M. Langer, "Taking into account wave effects in Monte Carlo simulation of phase contrast imaging using the Wigner distribution function," in *Unconventional Optical Imaging IV*, edited by I. Georgakoudi, M. P. Georges, and N. Verrier (International Society for Optics and Photonics, SPIE, 2024), Vol. 12996, p. 129960W.

[40] V. Arrizón, U. Ruiz, R. Carrada, and L. A. González, "Pixelated phase computer holograms for the accurate encoding of scalar complex fields," J. Opt. Soc. Am. A **24**, 3500–3507 (2007).
[41] J. R. Moore *et al.*, "The silicon backplane design for an LCOS polarization-insensitive phase hologram SLM," IEEE Photonics Technol. Lett. **20**, 60–62 (2008).
[42] M. Barbieri, "Optical quantum metrology," PRX Quantum **3**, 010202 (2022).
[43] L. Motka, B. Stoklasa, M. D'Angelo, P. Facchi, A. Garuccio, Z. Hradil, S. Pascazio, F. V. Pepe, Y. S. Teo, J. Řeháček, and L. L. Sánchez-Soto, "Optical resolution from Fisher information," Eur. Phys. J. Plus **131**, 130 (2016).
[44] S. Lawo, M. Hasegan, G. D. Gupta, and L. Pelletier, "Subdiffraction imaging of centrosomes reveals higher-order organizational features of pericentriolar material," Nat. Cell Biol. **14**, 1148–1158 (2012).